Journal of
Materials Chemistry A

ROYAL SOCIETY
OF CHEMISTRY

PAPER

View Article Online
View Journal | View Issue

Check for updates

Cite this: *J. Mater. Chem. A*, 2019, **7**, 6801

A nitrogen-containing all-solid-state hyperbranched polymer electrolyte for superior performance lithium batteries†

Lei Zhang,‡[b] Shi Wang,‡[a] Jingyu Li,[c] Xu Liu,[a] Pingping Chen,[a] Tong Zhao *[c] and Liaoyun Zhang *[a]

Received 6th January 2019
Accepted 18th February 2019

DOI: 10.1039/c9ta00180h

rsc.li/materials-a

Polyether-based materials, especially poly(ethylene oxide) (PEO) and derivatives thereof, have been extensively studied as Li-conducting all-solid-state polymer electrolytes (SPEs) for Li-based batteries due to their specific advantages such as easy fabrication, high safety, and outstanding compatibility with lithium salts. However, PEO-based polymers usually have too strong complexation ability with lithium ions and high crystallinity, resulting in a low lithium-ion transference number and room temperature ionic conductivity. In this study, we choose hyperbranched polyethylenimine (HPEI) as the core of a SPE matrix, while polyester segments as the arms through sequential ring-open polymerization (ROP) of glycolide (GC) and ε-caprolactone (CL). Specifically, the HPEI core containing N atoms can promote the dissociation of lithium salts, while the polyester segments can effectively dissolve lithium salts and transport ions. Furthermore, the SPE (HPEI–PGC–PCL/LiTFSI) is cast onto a ceramic film containing ceramic nanowires to prepare a composite SPE (CSPE), which can further construct ion transport channels at the interface of the polymer and nanowires. Synergizing the advantages of HPEI–PGC–PCL and ceramic nanowires, the CSPE exhibits superior electrochemical performance. Especially, the $LiFePO_4$/CSPE/Li cell exhibits a discharge capacity of 162 mA h g^{-1} at the C-rates of 0.2, 0.5 and 1C, and an average discharge capacity of 158 mA h g^{-1} with an average coulombic efficiency of 99.8% over 200 cycles at 0.5C. More importantly, the $LiCoO_2$/CSPE/Li cell also shows very good cycling performance (reaches 130 mA h g^{-1} at a current density of 0.06 mA cm^{-2}) and rate capacity (reaches 80 mA h g^{-1} at a current density of 0.3 mA cm^{-2}). This work highlights a new and novel host material that has the potential to be used as a high performance all-solid-state electrolyte for solid-state batteries.

Introduction

Polyether-based materials (especially poly(ethylene oxide) (PEO) and its derivatives) show many advantages when used as an all-solid-state polymer electrolyte (SPE) matrix, such as good electrochemical stability, low cost, easy fabrication, high safety, and superior compatibility with lithium salts, which makes them become one of the most promising candidates of SPE matrices for next generation high safety and high energy density lithium-ion batteries (LIBs).[1–3] Therefore, a vast majority of studies about solid-state electrolytes are based on PEO/PEO-based derivatives.[4–7] However, the high crystallinity of PEO usually results in the low room temperature ionic conductivity of the related SPE. Furthermore, it is reported that PEO-based SPEs generally show a low lithium-ion transference number due to the rather stable coordination structure between PEO and Li^+.[8,9] Obviously, such problems limit the application of polyether materials in solid-state LIBs. Therefore, it is very necessary look for alternative materials as polymer electrolytes. Meanwhile, development of new solid state electrolytes with excellent electrochemical performance is also very meaningful.[10–13]

It is suggested that a polymer backbone containing N atoms can decrease the binding energies of cations/anions, which is beneficial to the dissociation of lithium salts.[14,15] Moreover, compared with O atoms, N atoms generally are a better donor.[16] Therefore, electrolytes using polyethyleneimine (PEI, containing high contents of N atoms) and its derivatives as matrices have been paid much attention.[17–20] Of particular interest, hyperbranched PEI (HPEI) has more favorable properties when

---

[a] *School of Chemical Sciences, University of Chinese Academy of Sciences, Beijing 100049, China. E-mail: zhangly@ucas.ac.cn*

[b] *College of Science, China University of Petroleum-Beijing, Beijing 102249, China*

[c] *Laboratory of Advanced Polymer Materials, Institute of Chemistry, Chinese Academy of Sciences, Beijing 100190, China. E-mail: tzhao@iccas.ac.cn*

† Electronic supplementary information (ESI) available: Preparation of the ceramic membrane containing the ceramic nanowires, picture and XRD of the ceramic membrane (Fig. S1), TGA curves of the series of the synthesized polymers and DSC curves of the series of the prepared polymers and the CSPE (Fig. S2), ^{1}H NMR of PCL and PCL–PGC (Fig. S3), ionic conductivity of the CSPE and PGC–PCL/30% LiTFSI/ceramic film (Fig. S4), related parameters of E_a and T_o (Table S1), and related parameters of t^+ (Table S2). See DOI: 10.1039/c9ta00180h

‡ Lei Zhang and Shi Wang contributed equally to this work.

compared with linear PEI because HPEI can form homogeneous amorphous salt complexes at much lower salt concentrations.[21] Moreover, compared with linear polymers, the unique topological structure itself has the advantages such as higher mobility in the outer sphere of arms and lower crystallinity of the branched matrix, which likely can improve the ionic conductivity of the corresponding SPE.[22,23]

Based on the advantages of HPEI, we try to use HPEI as the core of a hyperbranched polymer to construct a novel and high performance SPE matrix. Then, we need to introduce special arms at the end of HPEI to further improve the Li^+ transport ability of the SPE. Very recently, we synthesized a hyperbranched SPE matrix containing polyester segments,[24] which shows a high t^+ due to the overall weaker coordinating between Li^+ and carbonyl groups than that of groups in PEO and Li^+.[9,25] Hence, a novel total polyester chain, namely, poly(glycolide)–poly(ε-caprolactone) (PGC–PCL), attracts our attention.

To obtain a high performance SPE, in addition to the reasonable design of the structure of the polymer, another effective way to reach the goal is compositing the SPE with ceramic nanofillers, especially ceramic nanowires because the interface between the polymer and nanowires can provide fast ion transport channels for more efficient conduction of ions.[26,27]

In this study, a novel HPEI-based SPE matrix containing total polyester chains (PGC–PCL) is synthesized *via* sequential ring opening polymerization (ROP) of glycolide (GC) and ε-caprolactone (CL) while using HPEI as the initiator. Specifically, the HPEI core containing N atoms can promote the dissociation of lithium salts, while the polyester segments also can effectively dissolve lithium salts and transport ions. To the best of our knowledge, such a SPE (HPEI–PGC–PCL/LiTFSI) has not been reported. Moreover, the SPE is cast onto a ceramic film containing ceramic nanowires to prepare a composite SPE (CSPE), in which the ion transport channels are further constructed at the interface between the polymer and nanowires. Synergizing the advantages of HPEI–PGC–PCL and ceramic nanowires, the CSPE exhibits excellent comprehensive electrochemical performances. As a result, both the $LiFePO_4$ (LFP)/CSPE/Li and $LiCoO_2$ (LCO)/CSPE/Li cells exhibit superior cycling performance and rate capacity. This work highlights a host material that has the potential to replace PEO-based polymers for high performance all-solid-state electrolytes used in LIBs.

Results and discussion

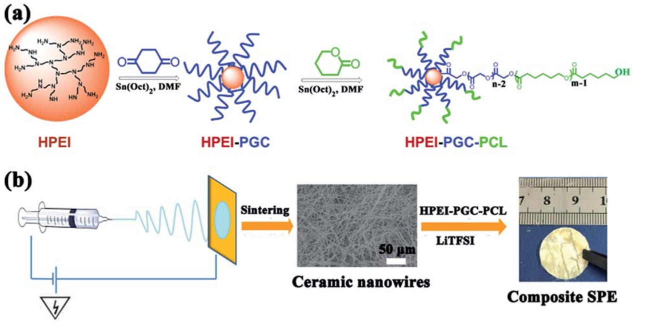

Scheme 1 (a) Schematic diagram of the synthesis route of the all-solid-state hyperbranched polymer matrix (HPEI–PGC–PCL). (b) The schematic illustration of the preparation process of the ceramic film containing ceramic nanowires and the CSPE.

Considering that most of the SPE matrices are PEO-based polymers, a new polymer using hyperbranched polyethylenimine as the core is designed and synthesized. Scheme 1a shows the synthesis route of HPEI–PGC–PCL. Specifically, HPEI–PGC was obtained *via* ROP of GC using $Sn(Oct)_2$ as the catalyst and HPEI as the initiator. Subsequently, HPEI–PGC–PCL was synthesized *via* ROP of CL using $Sn(Oct)_2$ as the catalyst and HPEI–PGC as the initiator. To obtain the CSPE, HPEI–PGC–PCL/30 wt% LiTFSI was cast on a ceramic film and dried (Scheme 1b). We used ^1H NMR (Fig. 1) to characterize the series of the hyperbranched polymers. Fig. 1a presents the ^1H NMR of HPEI, and the peaks between 2.5 and 2.8 ppm belong to the proton signals of $-NH_2$ and –NH–. After ROP of GC, the ^1H NMR of HPEI–PGC in Fig. 1b shows that new peaks at 4.12 ppm (peak a), 4.63 ppm (peak c), 4.77–4.98 ppm (peak b) and 5.51 ppm (peak d) appear, suggesting that PGC segments have been attached to the core of HPEI. Furthermore, the peaks belonging to the core of HPEI shift from 2.5–2.8 ppm to 2.71–2.95 ppm, indicating that the attachment of PGC segments onto the HPEI influences the chemical shift of protons of the core. In addition, comparing the integral of methene protons connected to the terminal –OH of PGC segments (peak c at 4.63 ppm) with those in the segments of PGC (a and b peaks at 4.12 and 4.77–4.98 ppm, respectively), the degree of polymerization ($DP_{n(arm)}$, $DP_{n(arm)} = 12$) can be obtained using eqn (1):

$$DP_{n(arm)} = [I(a) + I(b) + I(c)]/I(c) \qquad (1)$$

The ^1H NMR of HPEI–PGC–PCL is also exhibited in Fig. 1c. Specifically, the characteristic proton peaks belonging to the core HPEI appear at 2.85–3.00 ppm, while the proton characteristic peaks at 4.15 ppm (peak a), 4.59 ppm (peak b) and 4.71 ppm (peak c) come from the segments of PGC. Especially, after attaching PCL segments onto HPEI–PGC, highly intensive

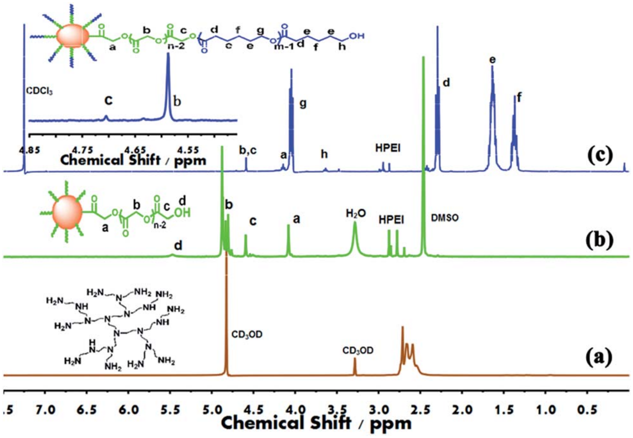

Fig. 1 ^1H NMR of (a) HPEI, (b) HPEI–PGC and (c) HPEI–PGC–PCL.

characteristic proton peaks arising from the PCL chain well appear (peaks from 1.71 to 1.30 ppm belong to $-CH_2-CH_2-CH_2-$, the peak at 2.29 ppm comes from $-CO-CH_2-$ and the peak at 4.05 ppm belongs to $-CH_2-O-CO-$). Thus, the ^{1}H NMR characterization indicates that HPEI–PGC–PCL has been synthesized *via* sequential ROP. Similarly, according to the ^{1}H NMR of HPEI–PGC–PCL, the $DP_{n(arm)}$ of the PCL segments is calculated to be 48.

We used IR spectra (Fig. 2) to further characterize the structural information of the series of the topological polymers. As shown in Fig. 2a (spectrum of HPEI), the stretching vibration at 3300 cm^{-1} belongs to the group of $-NH_2/-NH-$. The saturated $-CH_2-$ shows stretching vibration peaks in the range of 2990 to 2753 cm^{-1}. Meanwhile, the characteristic absorption peaks at 1596 and 1341/1286 cm^{-1} come from –NH– and –C–N–, respectively. Fig. 2a also shows the IR spectrum of HPEI with 30 wt% LiTFSI. In the IR spectra, the obvious difference between the spectra of HPEI and HPEI/LiTFSI is that the two characteristic absorption peaks belonging to –C–N– in the spectrum of HPEI change to only one peak in the spectrum of HPEI/LiTFSI. Meanwhile, the peak shifts to 1352 cm^{-1} in the IR spectra of HPEI/LiTFSI, strongly demonstrating that N atoms in –C–N– have effective interaction with Li^+.

After attaching PGC segments onto HPEI (Fig. 2b, spectrum of HPEI–PGC), new peaks such as –C(O)– (carbonyl group of the ester) and –C–O–C– appear at 1746–1650 and 1181 cm^{-1}, respectively. The IR spectrum of HPEI–PGC–PCL also shows the –C(O)– (ester group) and –C–O–C– peaks at 1721 and 1181 cm^{-1}, respectively. Interestingly, the characterize peak belonging to –NH–/–OH shows relatively low intensity at 3489 cm^{-1}, which is likely due to the high contents of PGC–PCL segments. The characterize peak belonging to –NH–/–OH shows higher intensity after adding LiTFSI into the hyperbranched polymer electrolyte matrix (HPEI–PGC–PCL). Moreover, compared with the polymer electrolyte matrix, a new peak arises at 1669 cm^{-1} due to the interaction of the ester group with lithium ions.[28,29] Such interaction is beneficial to the dissociation of LiTFSI. In addition, it is also observed that the peak belonging to –C–N– at 1365 cm^{-1} shifts to 1352 cm^{-1} after adding the lithium salt into HPEI–PGC–PCL, indicating that the core still has interaction with the lithium salt. According to the IR spectra, it is demonstrated that both the HPEI core and the polyester segments have strong interaction with the lithium salt, which is beneficial to the dissociation of LiTFSI. Thus, the ionic transport performance can likely be improved. From the ^{1}H NMR and IR characterization, it is also safe to conclude that the HPEI–PGC–PCL has been successfully synthesized.

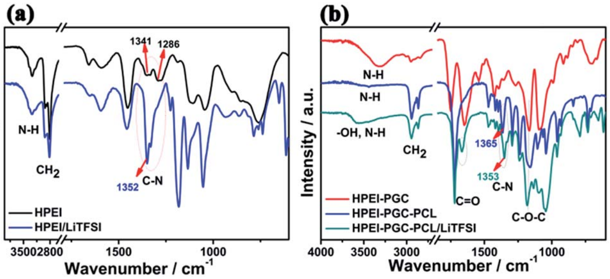

Fig. 2 (a) IR spectra of HPEI and HPEI/LiTFSI (30 wt%). (b) IR spectra of HPEI–PGC, HPEI–PGC–PCL and the SPE.

To replace organic liquid electrolytes and separators, the dried solid electrolyte needs to have good thermal performance. The thermal properties of the series of the topological polymers were further evaluated based on TGA (Fig. S2a and b†) and DSC (Fig. S2c†). As shown in Fig. S2a,† the T_{onset} of HPEI–PGC–PCL is 324 °C, indicating the very good thermal stability of the hyperbranched polymer electrolyte matrix. The DSC curves of the series of the polymers are presented in Fig. S2c.† Compared with the T_g (−51 °C) of HPEI, HPEI–PGC has a much higher T_g of −9 °C, which is likely because PGC segments are more rigid than PEI segments (the ability of the segments to move is reduced). A much high melting peak at 51 °C is observed in the DSC curve of HPEI–PGC–PCL due to the characteristic of easy crystallization of PCL segments. Addition of the lithium salt (LiTFSI) causes the obvious decrease of the melting peak. This is because a specific concentration of the lithium salt has a plasticizing effect, which is consistent with our previous reports.[22]

The microtopography of a ceramic film is exhibited in Fig. 3a (the ceramic film was prepared *via* electrostatic spinning, see the method in the ESI†). It is seen that the film is composed of equally distributed ceramic nanowires, while the nanowires have a diameter of about 300 nm (Fig. 3b). The surface microtopography of the CSPE is further presented in Fig. 3c and d at different magnifications. The SEM images of the CSPE indicate that the polymer electrolyte is uniformly coated on the surface of the ceramic film. In addition, Fig. 3e, f and g show the elemental distribution mappings of Al, O, and S of the CSPE, respectively (the inset of Fig. 3e presents the original SEM image

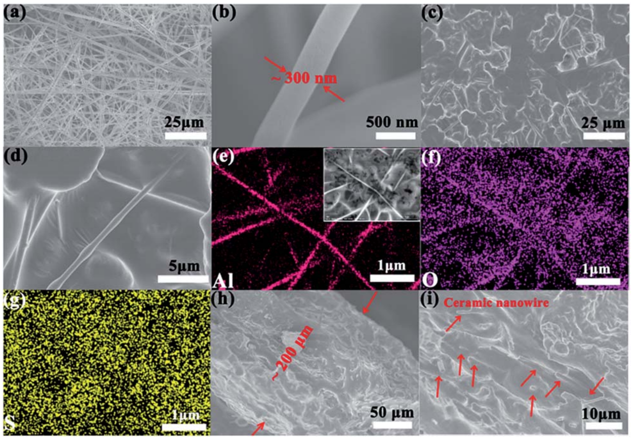

Fig. 3 (a) The SEM image of alumina ceramic nanowires. (b) A single ceramic nanowire with a diameter of ∼300 nm. (c) The surface morphology of the alumina electrostatic spinning film/hyperbranched polymer electrolyte (HPEI–PGC–PCL/LiTFSI) composite electrolyte, which indicates that the alumina film is uniformly coated by the SPE. (d) SEM image of the composite electrolyte film at a higher magnification (compared with (c)). (e), (f) and (g) show the elemental distribution mappings of Al, O, and S of the CSPE, respectively. Especially, the inset of (e) presents the original SEM image that is used to obtain the mappings. (h) and (i) show the cross section of the CSPE at different magnifications.

that is used to obtain the mappings). The elemental mappings further demonstrate that the HPEI-based polymer is composited with the ceramic film very well and the lithium salt is well embedded in the polymer matrix. To further confirm the above conclusions, the cross section of the CSPE is presented in Fig. 3h. Obviously, the polymer electrolyte uniformly fills the spaces between the nanowires. At a higher magnification (Fig. 3i), it can be clearly seen that the ceramic nanowires are uniformly filled by the HPEI-based polymer electrolyte on the cross section. Therefore, a new composite polymer electrolyte with the hyperbranched polyethylenimine-based polymer electrolyte containing total polyester segments is fabricated.

For all-solid-state electrolytes, one of the crucial parameters which needs to be evaluated is the ionic conductivity. Fig. 4a presents the ionic conductivity of the CSPE from 30 to 80 °C. As predicted, the ionic conductivity increases with the increase of temperature due to the stronger movement ability of the polymer segments and higher dissociation degree of the lithium salt.[30] Especially, the ionic conductivity of the CSPE reaches 2.66×10^{-5} and 5.36×10^{-4} S cm^{-1} at 30 °C and 80 °C, respectively. Here, we try to understand the ion transport mechanism of the CSPE. First, we compared the ionic conductivity of the CSPE and HPEI-based polymer electrolyte (without ceramic nanowires and the other conditions were the same) at 30 °C. As shown in Fig. 4b (the insets also show the impedance spectra of the two samples), it is found that the CSPE shows a much higher ionic conductivity (1.85 times) than the sample without ceramic nanowires, indicating the positive effect of ceramic nanowires on improving the ionic conductivity of the HPEI-based polymer electrolyte. It is believed that addition of ceramic nanofillers can reduce the crystallization of the polymer, resulting in the improvement of ionic conductivity.[31] However, comparing the XRD pattern of HPEI–PGC–PCL/LiTFSI with that of the CSPE, the crystalline peaks of the CSPE at 21–24° do not decrease, suggesting that the ceramic nanowires have no obvious influence on HPEI–PGC–PCL crystallinity. Therefore, the improved ionic conductivity of the CSPE should not belong to nanowire reduced crystallization. It is reported that a fast ion transport pathway can be constructed using ceramic nanowires, which likely is the reason for the improved ionic conductivity of the CSPE.[26,27]

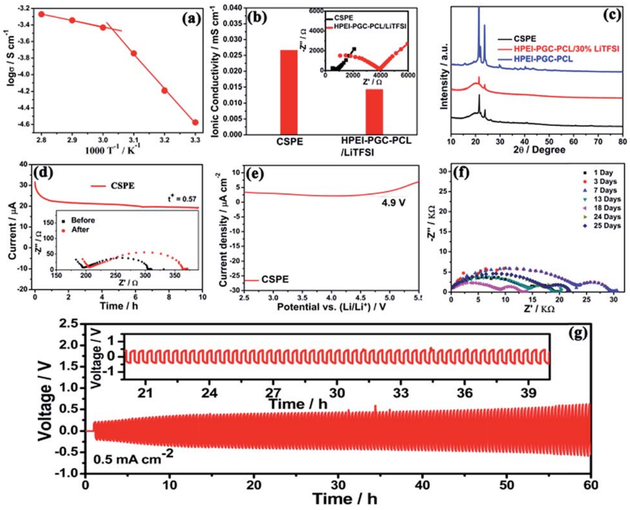

Fig. 4 (a) Ionic conductivity of the CSPE film at a given temperature (from 30 to 80 °C). (b) Comparison of the room temperature ionic conductivity of the CSPE and HPEI–PGC–PCL/30 wt% LiTFSI. The insets show the corresponding impedance spectra. (c) XRD profiles of the polymer matrix (HPEI–PGC–PCL), polymer electrolyte (HPEI–PGC–PCL/30 wt% LiTFSI) and CSPE. (d) Chronoamperometry of the Li/CSPE/Li symmetric cell at a potential step of 10 mV (conducted at 60 °C). The inset presents the AC impedance spectra before and after polarization at 60 °C. (e) Linear sweep voltammogram of a Li/CSPE/SS cell. (f) Impedance spectra of the CSPE after different storage times. (g) The potential profiles of repeated Li plating and striping using the CSPE with a current density of 0.5 mA cm^{-2} at 60 °C. The inset presents the selected potential profiles.

On the other hand, we also tried to explore the important role of the HPEI core in improving the ionic conductivity. Therefore, we compared the ionic conductivity of CSPE with that of PGC–PCL/ceramic film/30 wt% LiTFSI (see the ^{1}H NMR of PGC–PCL in the ESI†). As shown in Fig. S4,† the composite electrolyte based on PGC–PCL shows obviously low ionic conductivity in the whole temperature range compared with the CSPE, suggesting that HPEI also has a crucial role in improving the ionic conductivity. This is because the HPEI backbones contain high contents of N atoms that can promote ion-pair dissociation (this is also confirmed by the IR spectra in Fig. 2).[15,32] Moreover, compared with O atoms of PEO, the interaction between N atoms of HPEI and Li^+ is lower, which is more beneficial to the transport of carriers.

In addition, lithium ions usually hop in the polymer electrolytes decoupled with the movement of polymer segments at a temperature below the melting point, which can be described by using the Arrhenius model. However, lithium ions generally migrate along polymer chains at a temperature above the melting point, which obeys the Vogel–Tammann–Fulcher (VTF) model.[33] In this study, the experimental data in Fig. 4a are fitted *via* the Arrhenius model and VTF model at low temperature (crystalline phase) and high temperature (amorphous phase), respectively. Table S1† also shows the related fitting parameters of the models. As predicted, the activation energy ($E_{\text{a VTF}} = 4.16$ kJ mol^{-1}) of the VTF model is much lower than that of the Arrhenius model ($E_{\text{a Arrhenius}} = 34.53$ kJ mol^{-1}) due to the higher chain motion ability and dissociation degree of LiTFSI at higher temperature. According to the two fitting curves, a crossing point can be obtained, which corresponds to a temperature of the crystalline transition temperature (57 °C). Meanwhile, the phase transition temperature is ~50 °C according to the DSC test (Fig. S2b†), which is generally consistent with the fitting result.

Ionic conductivity is determined by both anion and cationic conduction. It is very crucial whether or not it is cationic conduction. One effective method is to evaluate the lithium-ion transference number (t^+) of the CSPE. The t^+ for the CSPE was tested and calculated using the following equation

$$t^+_{\text{Li}} = \frac{I_s(\Delta V - I_0 R_{l0})}{I_0(\Delta V - I_s R_{ls})} \quad (2)$$

where I_s and I_0 represent the steady and initial-state currents. R_{l0} and R_{ls} are the initial and steady resistances (Ω) of the passivation layer, respectively. ΔV is the voltage applied across the Li/CSPE/Li cell. The inset of Fig. 4d shows the impedance spectra before and after polarization of the CSPE while the current–time curve is also presented in Fig. 4d (Table S2† shows the related parameters). Subsequently, a t^+ of ~0.57 is obtained, which is very high compared with most of the reported SSEs.[34–37] Three reasons can explain the high t^+ of the CSPE. First, it has been recognized that the hyperbranched structure of polymer electrolyte matrices with flexible terminal segments have better ability to promote the transport of ions (compared with linear polymers).[22,38] Second, it should be noted that the polymer matrix we used is a hyperbranched polyethylenimine-based polymer. The high contents of N atoms in the polymer backbone can reduce the anion/cation binding energies, promoting dissociation of the lithium salt,[15] which likely can promote the transport of lithium ions. Furthermore, it has been demonstrated that addition of ceramic nanofillers can increase the t^+ because of the surface interactions between the polymer/lithium salt and ceramic fillers.[27] Specifically, the ceramic nanowires help to dissociate LiTFSI and then more free lithium ions are released.[26] Synergizing the interaction of nitrogen atoms and ceramic nanowires with the lithium salt results in high t^+ (the generally weaker coordinating between Li^+ and carbonyl groups than that of groups in PEO and Li^+ might also be a very crucial factor).

It is also significantly important to assess the electrochemical stability of a SSE. Fig. 4e shows the linear sweep voltammogram (LSV) of the Li/CSPE/SS cell at a scan rate of 5 mV s^{-1}. According to the LSV, the electrochemical window of the CSPE is 4.9 V, which is high enough to match various cathodes such as LFP and LCO-based cathodes.

Next, we present the AC impedance spectra of Li/CSPE/Li after different storage times in Fig. 4f. The diameter of capacitive arcs (at the real part) in the impedance spectra at high frequency represents the bulk resistance of the CSPE film. Meanwhile, the semicircle at intermediate frequency signifies the interface resistance (R_i) of the CSPE with electrodes. It is seen that R_i increases and then decreases to a stable value (~4 kΩ after storage for 18 days) with the increase of storage time, confirming that the compatibility of the CSPE with Li electrodes is good and also a stable passivation film has been constructed on the Li electrodes.[39]

The lithium plating/stripping experiments were conducted at a current density of 0.5 mA cm^{-2} with a charge/discharge time of 2 h at 60 °C to explore the ability of CSPE to inhibit lithium dendrites. As shown in Fig. 4g, the average overpotential of the Li/Li cell using the CSPE is ~90 mV and remains relatively stable after 60 h of cycling, suggesting that the CSPE has the ability to resist the growth of lithium dendrites.

Up to date, it should be noted that the widely used cathode of solid LIBs (especially PEO-based solid LIBs) has been based on LFP due to its relatively low charging voltage (4 V). It is still a great challenge to match SPEs with high-voltage cathodes such as LCO-based cathodes. Fortunately, the as-prepared CSPE with the above superior comprehensive electrochemical performance should be able to pair with high-voltage cathodes and lithium metal anodes to obtain LIBs with excellent performance (see below for the cell properties of the LFP/Li and LCO/Li cells using the CSPE).

To confirm that the CSPE can be applied to LIBs in practice, first, we assembled a LFP/CSPE/Li coin cell to evaluate the performance of the solid-state cell. Specifically, Fig. 5a exhibits the charge–discharge curves of the cell at C-rates from 0.2 to 2C. It is amazing to find that the discharge capacity is kept at 162 mA h g^{-1} at the C-rates of 0.2, 0.5 and 1C with only slightly increased overpotential with the increase of current density due to the polarization effect. Upon further increasing the current density to 2C, the discharge capacity still can reach ~140 mA h g^{-1}, further demonstrating the excellent rate property of the HPEI-based composite all-solid-state polymer electrolyte. The cycling performance of the solid-state cell at the corresponding C-rate (from 0.2 to 2C) is presented in Fig. 5b. It is clearly seen that charge and discharge capacity values are almost coincident, indicating the extremely high coulombic efficiency of the solid-state cell at different C-rates. Furthermore, once the C-rate is changed from 2 to 1C, the capacity is almost the same as the original 1C, confirming the superior reversibility of the cell.

Long-term cycling stability as well as high coulombic efficiency is also very crucial for a solid-state cell to be practically used. After the high C-rate cycling (0.2 to 2C), the cell is continuously used to evaluate the long-term cycling performance and coulombic efficiency at 0.5C (Fig. 5c, continuation of Fig. 5b). It is clearly seen that the cell has an average discharge capacity of 158 mA h g^{-1} with an average coulombic efficiency of 99.8% over 200 cycles, highlighting the excellent cell performance using the HPEI-based CSPE.

For all-solid-state electrolytes, it is well known that the corresponding solid-state LCO/Li cell cannot have good cycling

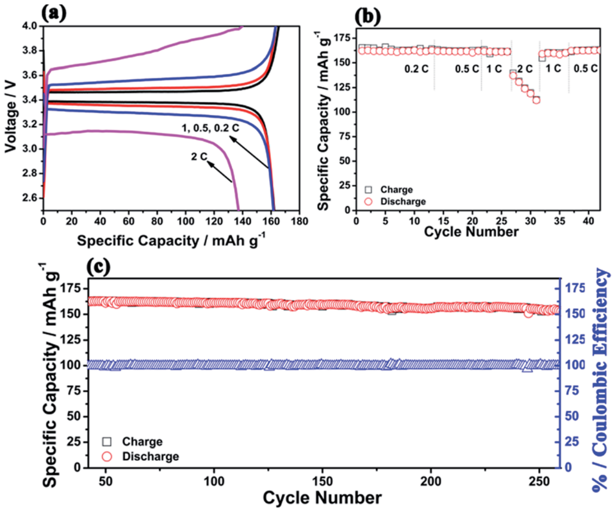

Fig. 5 (a) Charge–discharge curves of a LFP/CSPE/Li cell at different current densities. (b) Cycling performance of the all-solid-state LFP/Li cell using the CSPE film at C-rates from 0.2 to 2C. (c) Long-term cycling performance of the LFP/CSPE/Li cell at 0.5C after the high rate cycling (continuation of (b)). The experiment was conducted at 60 °C.

performance and rate capacity due to the less stability of the LCO-based cathode than that of the LFP-based cathode. In the next step, we focused our attention on the cell performance of the LCO/CSPE/Li cell and the voltage range was set from 3 to 4.3 V because of the high electrochemical window of the CSPE (4.9 V). On the other hand, for the practical use of SSEs, the active substance content of the cathode needs to be increased, so the energy density of the cell can be increased. Therefore, in this study, the active substance content of the LCO-based cathode was increased to ~4.5 mg cm^{-2} (the active substance contents are usually limited to 1–2 mg cm^{-2}). Fig. 6a shows the charge–discharge curves of the LCO/CSPE/Li cell at different cycles, and the first discharge capacity reaches 130 mA h g^{-1} and the overpotential remains stable at different cycles. The corresponding cycling performance of the cell at 0.1C is shown in Fig. 6b. It can be seen that the discharge capacity is still higher than 100 mA h g^{-1} after 50 cycles and the coulombic efficiency of the cell is increased from ~90% at the first cycle to ~100% after 5 cycles. We further evaluated the rate capacity of the LCO/CSPE/Li cell under different C-rates. Fig. 6c is the typical charge–discharge curves of the cell at the C-rates of 0.1, 0.2 and 0.5C. With the increase of current density, the overpotential increases due to the polarization effect. It is clearly seen in Fig. 6d that the discharge capacity reaches 80 mA h g^{-1} at 0.5C. However, the discharge capacity slightly decreases once the current density returns to 0.2 and 0.1C, which is likely because of the relatively poor cycling stability of the LCO-based cathode.

Generally, we have confirmed that the HPEI-based CSPE exhibits excellent cycling performance and rate capacity using LFP-based and LCO-based cathodes. The superior cell performance is attributed to the reasonable ionic conductivity and the high t^+ value, which is obtained by synergizing the effective dissociation of the lithium salt based on the HPEI core containing high contents of N atoms, effective transport of Li ions using polyester segments, and construction of ion channels at the interface between the polymer matrix and ceramic nanowires.

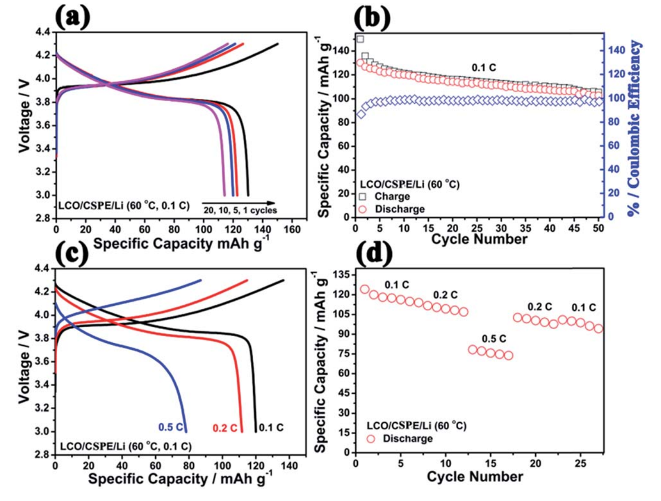

Fig. 6 (a) Charge and discharge curves of a LCO/CSPE/Li cell at 0.1C at different cycles. (b) Cycling performance of the LCO/Li cell using the CSPE film at 0.1C. (c) Charge and discharge curves of a LCO/CSPE/Li cell at different C-rates. (d) Cycling performance of the LCO/Li cell using the CSPE film at the C-rates of 0.1, 0.2 and 0.5C.

Conclusions

Using hyperbranched PEI as the core, we prepared a new hyperbranched PEI-based all-solid-state polymer electrolyte matrix containing total polyester segments *via* sequential ROP using glycolide and ε-caprolactone as monomers. Specifically, the hyperbranched PEI core containing N atoms could reduce the anion/cation binding energies and promote the dissociation of lithium salts. Meanwhile, the polyester segments were beneficial to transporting lithium ions. Addition of ceramic nanowires further promoted the dissociation of lithium salts, and the surface interactions between the polymer/lithium salt and ceramic nanowires could act as ion transport channels. As a result, the CSPE exhibited superior comprehensive electrochemical performance, such as a high room temperature ionic conductivity (2.66×10^{-5} S cm^{-1}), outstanding t^+ (~0.57), wide electrochemical window (4.9 V), and good compatibility with Li metal. More importantly, the LFP/Li cell using the CSPE not only presented superior rate capacity (discharge capacity was maintained at 162 mA h g^{-1} at the C-rates of 0.2, 0.5 and 1C) but also showed excellent long-term cycling performance (average discharge capacity of 158 mA h g^{-1} with an average coulombic efficiency of 99.8% over 200 cycles). Furthermore, the LCO/CSPE/Li cell also exhibited very good cycling performance and rate capacity under a high active substance content (~4.5 mg cm^{-2}) of the cathode. This study provides a new kind of CSPE (using a nitrogen-containing hyperbranched polymer as a matrix) for high performance all-solid-state high-voltage lithium batteries, which has the potential to be applied in next generation high energy density maintaining power devices.

Experimental

Materials

Hyperbranched polyethylenimine (HPEI, Aldrich, M_n = ~10 000 g mol^{-1}), tin(II) 2-ethylhexanoate (95%, Aladdin), glycolide (GC, 99%, Macklin) and bis(trifluoromethane)sulfonimide lithium (LiTFSI, 99%, Aladdin) were used as received. *N*,*N*′-Dimethyl formamide (DMF, AR, Beijing Chemical Works) and ε-caprolactone (CL, 99%, Alfa Aesar) were dried with CaH_2 and distilled prior to use.

Synthesis of the hyperbranched polymer electrolyte matrix

HPEI–PGC was obtained *via* ROP using GC as the monomer and HPEI as the initiator ($Sn(Oct)_2$ used as the catalyst). Subsequently, HPEI–PGC–PCL was synthesized by further ROP of HPEI–PGC and CL while using $Sn(Oct)_2$ as the catalyst.

Synthesis of HPEI–PGC

Typically, HPEI (0.54 g, 9.16 mmol of primary and secondary amine groups), GC (1.775 g, 15.30 mmol), DMF (10 mL) and

$Sn(Oct)_2$ (0.24 g, 0.59 mmol) were placed in a dry round-bottom flask. The reaction unit was degassed by three freeze–pump–thaw cycles. Then, the polymerization was performed at 135 °C for 24 h. After the reaction, DMF was removed by reduced pressure distillation. Subsequently, brown HPEI–PGC was obtained by washing the mixture with methanol and drying in a vacuum oven at 50 °C for 24 h.

Synthesis of HPEI–PGC–PCL

In a typical experiment, HPEI–PGC (0.3 g) and $Sn(Oct)_2$ (0.020 g, 0.050 mmol) were added into a dry round-bottom flask. Toluene (2 mL) was added into the reaction unit and then distilled before DMF (10 mL) was added under a N_2 atmosphere. After temperature was raised up to 130 °C, CL (5 mL) was slowly added to the mixture. The mixture was stirred vigorously for 24 h at 130 °C. After cooling, the mixture was precipitated in excess methanol. The product (HPEI–PGC–PCL, a light yellow powder) was obtained by filtration and dried in a vacuum at 50 °C for 24 h.

Preparation of the HPEI-based composite all-solid-state polymer electrolyte (CSPE)

LiTFSI (0.3 g) and HPEI–PGC–PCL (3 g) were dissolved in THF (5 mL). The solution was added dropwise on the surface of a free-standing aluminium oxide ceramic electrostatic spinning film containing the ceramic nanowires. Subsequently, the composite film was dried at 50 °C under vacuum conditions for 24 h to obtain the CSPE.

Characterization

The FTIR spectra were obtained using a Thermo Nicolet AVATAR 360 infrared instrument with an attenuated total reflectance (ATR) attachment, and the range of scanning wave numbers was from 4000 to 500 cm^{-1}. The structural information (^1H NMR spectra) of the hyperbranched polymers was characterized *via* a JNM-ECZ400S (JEOL, 400 MHz) spectrometer. SEM images and EDX data were obtained using a Hitachi SU8010 Field Emission Scanning Electron Microscope (FESEM) with an EDX detector. The samples were sputtered with Au for 30 s. Differential scanning calorimetry (DSC) tests were conducted using a TA Instrument Q2000. During the DSC measurements, an empty reference aluminum pan and pans containing samples ($\sim$5 mg) with lids were heated from room temperature to 150 °C at a rate of 10 °C min^{-1} and then cooled to -90 °C at a rate of 10 °C min^{-1} under a N_2 atmosphere. The DSC data used were the second heating traces. A Perkin-Elmer TGA 1 series instrument was used to analysis the thermal stabilities of the series of the polymers with a heating rate of 20 °C min^{-1} from 50 to 600 °C under a N_2 atmosphere.

Electrochemical measurements

The CSPE was sandwiched between two stainless steel (SS) blocking electrodes to measure the ionic conductivity using electrochemical impedance spectroscopy. The Li-ion transport number was calculated by alternating current (AC) impedance and direct-current (DC) polarization measurement using a Li/CSPE/Li symmetric cell. The electrochemical stability window of the CSPE was obtained by using a Li/CSPE/SS coin cell using a Zahner-Zennium electrochemical workstation. The detailed information can be found in our previous reports.[22,24,40]

Furthermore, both LFP-based and LCO-based cathodes were used to evaluate the cell performance of the CSPE. Both LFP and LCO were kindly provided by Pulead Technology Industry Co., Ltd. For the LFP-based cathode, the active substance content was 1.5–2.5 mg cm^{-2}, while the LCO-based cathode contained an active substance content of 4–5 mg cm^{-2}.

In addition, the LFP-based cathode consisted of LFP (70 wt%), super P (20 wt%) and PVDF (10 wt%). The LCO-based cathode included LCO (90 wt%), super P (5 wt%) and PVDF (5 wt%). The LFP/CSPE/Li and LCO/CSPE/Li cells were assembled in an Ar-filled glovebox (MB-Labstar 1200/780) with H_2O and O_2 contents lower than 0.5 ppm. A LANHE CT2001A battery testing system was used to measure the cell performances of all the all-solid-state batteries. Specifically, the LCO/CSPE/Li cells were galvanostatically charged and discharged between 3 and 4.3 V while the cells were run at 60 °C. The charge and discharge ranges of the LFP/CSPE/Li cells were between 2.5 and 4 V and the cells were also run at 60 °C.

Conflicts of interest

There are no conflicts to declare.

Acknowledgements

We acknowledge the help from the Analysis and Testing Center at the University of Chinese Academy of Sciences. The authors also acknowledge the support of the National Natural Science Foundation of China (No. 51073170) and Innovation Program of CAS Combination of Molecular Science and Education.

Notes and references

1 E. Quartarone and P. Mustarelli, *Chem. Soc. Rev.*, 2011, **40**, 2525–2540.
2 Z. Xue, D. He and X. Xie, *J. Mater. Chem. A*, 2015, **3**, 19218–19253.
3 T. F. Miller III, Z.-G. Wang, G. W. Coates and N. P. Balsara, *Acc. Chem. Res.*, 2017, **50**, 590–593.
4 J. Bae, Y. Li, J. Zhang, X. Zhou, F. Zhao, Y. Shi, J. B. Goodenough and G. Yu, *Angew. Chem., Int. Ed.*, 2018, **57**, 2096–2100.
5 H. Duan, Y.-X. Yin, Y. Shi, P.-F. Wang, X.-D. Zhang, C.-P. Yang, J.-L. Shi, R. Wen, Y.-G. Guo and L.-J. Wan, *J. Am. Chem. Soc.*, 2018, **140**, 82–85.
6 S. Li, Y.-M. Chen, W. Liang, Y. Shao, K. Liu, Z. Nikolov and Y. Zhu, *Joule*, 2018, **2**, 1838–1856.
7 L. Long, S. Wang, M. Xiao and Y. Meng, *J. Mater. Chem. A*, 2016, **4**, 10038–10069.
8 O. Buriez, Y. B. Han, J. Hou, J. B. Kerr, J. Qiao, S. E. Sloop, M. M. Tian and S. G. Wang, *J. Power Sources*, 2000, **89**, 149–155.

9 J. Mindemark, M. J. Lacey, T. Bowden and D. Brandell, *Prog. Polym. Sci.*, 2018, **81**, 114–143.

10 J. Zhang, J. Zhao, L. Yue, Q. Wang, J. Chai, Z. Liu, X. Zhou, H. Li, Y. Guo, G. Cui and L. Chen, *Adv. Energy Mater.*, 2015, **5**, 1501082.

11 T. Dong, J. Zhang, G. Xu, J. Chai, H. Du, L. Wang, H. Wen, X. Zang, A. Du and Q. Jia, *Energy Environ. Sci.*, 2018, **11**, 1197–1203.

12 P. Hu, J. Chai, Y. Duan, Z. Liu, G. Cui and L. Chen, *J. Mater. Chem. A*, 2016, **4**, 10070–10083.

13 X. Zhang, T. Liu, S. Zhang, X. Huang, B. Xu, Y. Lin, B. Xu, L. Li, C.-W. Nan and Y. Shen, *J. Am. Chem. Soc.*, 2017, **139**, 13779–13785.

14 M. J. Erickson, R. Frech and D. T. Glatzhofer, *Polymer*, 2004, **45**, 3389–3397.

15 R. P. Doyle, X. Chen, M. Macrae, A. Srungavarapu, L. J. Smith, M. Gopinadhan, C. O. Osuji and S. Granados-Focil, *Macromolecules*, 2014, **47**, 3401–3408.

16 I. B. Pehlivan, P. Georen, R. Marsal, C. G. Granqvist and G. A. Niklasson, *Electrochim. Acta*, 2011, **57**, 201–206.

17 I. B. Pehlivan, C. G. Granqvist and G. A. Niklasson, *Electrochim. Acta*, 2014, **119**, 164–168.

18 Y. Zhang, J.-J. Yuan, Y.-Z. Song, X. Yin, C.-C. Sun, L.-P. Zhu and B.-K. Zhu, *Electrochim. Acta*, 2018, **275**, 25–31.

19 F. Pignanelli, M. Romero, R. Faccio and A. W. Mombru, *J. Phys. Chem. B*, 2017, **121**, 6759–6765.

20 I. B. Pehlivan, E. L. Runnerstrom, S. Y. Li, G. A. Niklasson, D. J. Milliron and C. G. Granqvist, *Appl. Phys. Lett.*, 2012, **100**, 127–492.

21 C. S. Harris, M. A. Ratner and D. F. Shriver, *Macromolecules*, 1987, **20**, 1778–1781.

22 S. Wang, A. Wang, C. Yang, R. Gao, X. Liu, J. Chen, Z. Wang, Q. Zeng, X. Liu and H. Zhou, *J. Power Sources*, 2018, **395**, 137–147.

23 J. M. Ren, T. G. McKenzie, Q. Fu, E. H. H. Wong, J. Xu, Z. An, S. Shanmugam, T. P. Davis, C. Boyer and G. G. Qiao, *Chem. Rev.*, 2016, **116**, 6743–6836.

24 S. Wang, A. Wang, X. Liu, H. Xu, J. Chen and L. Zhang, *Electrochim. Acta*, 2018, **259**, 213–224.

25 J. Mindemark, B. Sun, E. Törmä and D. Brandell, *J. Power Sources*, 2015, **298**, 166–170.

26 W. Liu, D. Lin, J. Sun, G. Zhou and Y. Cui, *ACS Nano*, 2016, **10**, 11407–11413.

27 W. Liu, S. W. Lee, D. Lin, F. Shi, S. Wang, A. D. Sendek and Y. Cui, *Nat. Energy*, 2017, **2**, 17035.

28 I. Osada, S. M. Hosseini, S. Jeong and S. Passerini, *ChemElectroChem*, 2017, **4**, 463–467.

29 I. D. Wu and F.-C. Chang, *Polymer*, 2007, **48**, 989–996.

30 W. Zhou, S. Wang, Y. Li, S. Xin, A. Manthiram and J. B. Goodenough, *J. Am. Chem. Soc.*, 2016, **138**, 9385–9388.

31 F. Croce, G. Appetecchi, L. Persi and B. Scrosati, *Nature*, 1998, **394**, 456.

32 B. Unal, R. J. Klein, K. R. Yocca and R. C. Hedden, *Polymer*, 2007, **48**, 6077–6085.

33 L. Yang, Z. Wang, Y. Feng, R. Tan, Y. Zuo, R. Gao, Y. Zhao, L. Han, Z. Wang and F. Pan, *Adv. Energy Mater.*, 2017, **7**, 1701437.

34 Y. Lin, X. Wang, J. Liu and J. D. Miller, *Nano Energy*, 2017, **31**, 478–485.

35 Q. Pan, D. M. Smith, H. Qi, S. Wang and C. Y. Li, *Adv. Mater.*, 2015, **27**, 5995–6001.

36 B. Chen, Q. Xu, Z. Huang, Y. Zhao, S. Chen and X. Xu, *J. Power Sources*, 2016, **331**, 322–331.

37 O. Sheng, C. Jin, J. Luo, H. Yuan, H. Huang, Y. Gan, J. Zhang, Y. Xia, C. Liang and W. Zhang, *Nano Lett.*, 2018, **18**, 3104–3112.

38 D. Marmorstein, T. Yu, K. Striebel, F. McLarnon, J. Hou and E. Cairns, *J. Power Sources*, 2000, **89**, 219–226.

39 K. Liu, F. Ding, J. Liu, Q. Zhang, X. Liu, J. Zhang and Q. Xu, *ACS Appl. Mater. Interfaces*, 2016, **8**, 23668–23675.

40 S. Wang, X. Liu, A. Wang, Z. Wang, J. Chen, Q. Zeng, X. Jiang, H.-H. Zhou and L. Zhang, *ACS Appl. Mater. Interfaces*, 2018, **10**, 25273–25284.